

Understanding the Preparation and Reactivity of Mo/ZSM-5 Methane Dehydroaromatization Catalysts

Yujie Liu,^[a] Hao Zhang,^[a] Alexandra S. G. Wijkema,^[a] Ferdy J. A. G. Coumans,^[a] Lingqian Meng,^[a] Evgeny A. Uslamin,^[a] Alessandro Longo,^[b, c] Emiel J. M. Hensen,^{*[a]} and Nikolay Kosinov^{*[a]}

Abstract: Methane dehydroaromatization is a promising reaction for the direct conversion of methane to liquid hydrocarbons. The active sites and the mechanism of this reaction remain controversial. This work is focused on the operando X-ray absorption near edge structure spectroscopy analysis of conventional Mo/ZSM-5 catalysts during their whole lifetime. Complemented by other characterization techniques, we derived spectroscopic descriptors of molybdenum precursor decomposition and its exchange with zeolite

Brønsted acid sites. We found that the reduction of Mo-species proceeds in two steps and the active sites are of similar nature, regardless of the Mo content. Furthermore, the ZSM-5 unit cell contracts at the beginning of the reaction, which coincides with benzene formation and it is likely related to the formation of hydrocarbon pool intermediates. Finally, although reductive regeneration of used catalysts via methanation is less effective as compared to combustion of coke, it does not affect the structure of the catalysts.

Introduction

Natural gas (>85% methane) is an essential feedstock for the production of energy, fuels, and chemicals owing to its high abundance and low price.^[1] The low volumetric energy density of methane makes its transport and utilization expensive.^[2] Liquefaction or pipeline transport are not economical for many remote and/or small gas fields. In this respect, it is necessary to develop efficient small-scale technologies to convert methane to high-value and easily transportable chemicals, such as liquid fuels or commodity chemicals.^[3]

Non-oxidative dehydroaromatization of methane (MDA) is one of the most promising reactions to directly convert methane to liquid aromatic hydrocarbons and H₂ gas as a valuable co-product. Zeolite-based Mo/ZSM-5 and Mo/MCM-22

are the most effective catalysts for the MDA reaction, typically displaying a benzene selectivity of 60–80% at a thermodynamically limited methane conversion of 10–12% at 700 °C.^[4] The three-dimensional channel structure, suitable pore diameter (5.5 Å), and the ease of synthesis make ZSM-5 zeolite the most extensively used support for MDA catalysts.^[5] While significant progress has been achieved, two major challenges have yet to be overcome – suboptimal benzene formation activity and rapid coking deactivation.^[6] To design better catalysts that will contribute to a more viable MDA process, it is essential to understand the nature of the active sites and the reaction mechanism.

Substantial efforts have already been devoted to determining the structure of Mo-species in the working catalysts. It is established that the as-prepared Mo/ZSM-5 contains dispersed Mo(VI)-oxo species, which are subsequently reduced and/or carburized by methane under reaction conditions. These reduced/carburized Mo-centers are believed to be responsible for methane activation.^[6,7] However, it remains debated whether Mo-carbide particles/clusters/single atoms or Mo-oxo cationic species stabilized on Brønsted acid sites are the actual active centers. For example, using high-resolution transmission electron microscopy (HRTEM), Matus et al.^[8] found that both large Mo₂C particles (2–15 nm) on the zeolite external surface and small Mo-containing clusters (~1 nm) located inside zeolite channels are formed during the MDA reaction. Using ultrahigh field ⁹⁵Mo nuclear magnetic resonance (NMR) spectroscopy, Zheng et al.^[9] obtained direct spectroscopic evidence for the formation of exchanged Mo-species interacting with framework Al sites. Furthermore, combining NMR results with catalytic data, the authors concluded that such exchanged Mo-oxo species are the precursors for the actual active centers. Vollmer et al.^[10] distinguished Mo-sites of different nature on Mo/ZSM-5 samples (1–5 wt.%) reduced in CO and CH₄ by means of infrared

[a] Y. Liu, H. Zhang, A. S. G. Wijkema, F. J. A. G. Coumans, Dr. L. Meng, Dr. E. A. Uslamin, Prof. E. J. M. Hensen, Dr. N. Kosinov
Laboratory of Inorganic Materials & Catalysis
Department of Chemical Engineering and Chemistry
Eindhoven University of Technology
P.O. Box 513, 5600 MB Eindhoven (Netherlands)
E-mail: e.j.m.hensen@tue.nl
n.a.kosinov@tue.nl

[b] Dr. A. Longo
European Synchrotron Radiation Facility
71 Avenue des Martyrs, 38000 Grenoble (France)

[c] Dr. A. Longo
Istituto per lo Studio dei Materiali Nanostrutturati (ISMN)-CNR
UOS Palermo, Via Ugo La Malfa, 153, 90146 Palermo (Italy)

Supporting information for this article is available on the WWW under <https://doi.org/10.1002/chem.202103894>

© 2021 The Authors. Chemistry - A European Journal published by Wiley-VCH GmbH. This is an open access article under the terms of the Creative Commons Attribution Non-Commercial NoDerivs License, which permits use and distribution in any medium, provided the original work is properly cited, the use is non-commercial and no modifications or adaptations are made.

spectroscopy of adsorbed CO (CO IR) combined with ^{13}C NMR and computational modeling. Two types of Mo-sites (mono- and dimeric (oxy-) carbidic species) dispersed inside the pores of the zeolite and larger Mo-carbide nanoparticles on the outer surface were proposed. The concentration of Mo-species on the external surface was low for Mo loading ≤ 2 wt.%, and significant for the 5 wt.% Mo/ZSM-5 catalyst. Altogether, the structure of the active Mo-sites in working catalysts remains debatable. It is also generally unclear how the structure of the active sites depends on the Mo loading, Si/Al ratio, and catalyst preparation method.

Quick deactivation of zeolite-based catalysts is another challenge. To render the MDA reaction commercially attractive, the rapid deactivation of Mo/ZSM-5 related to build-up of carbon deposits (coke) should be resolved. Removal of coke with O_2 ^[11] or H_2 ^[12] can be performed during regeneration of Mo/ZSM-5 catalysts. Besides, co-feeding of H_2 ^[13] O_2 ^[14] and oxygenates^[15] with the methane feed are known methods to suppress the formation of coke. The catalyst stability during regeneration steps is an important topic. In this respect we need to understand the structural evolution of Mo-sites during reductive and oxidative removal of coke.^[16]

X-ray absorption spectroscopy (XAS) has emerged as a powerful tool to study MDA catalysts. First of all, XAS is a bulk technique, and it is suitable for the analysis of the active species dispersed inside the zeolite pores.^[17] Second, the active sites only form under harsh reaction conditions ($\geq 650^\circ\text{C}$), accompanied by a significant amount of coke deposition. It makes the system difficult for operando characterization by X-ray photoelectron, UV-Vis, IR, Raman, and NMR spectroscopies. As transmission XAS at Mo K-edge (20.000 keV) is compatible with the high-temperature operando cells, it can be used to follow changes occurring under relevant reaction conditions.^[18] Third, XAS is sensitive to the small perturbations of structure and oxidation state of Mo.^[19] MDA is a complex reaction and several reaction stages can be distinguished: activation, induction, pseudo steady-state reaction, deactivation, and eventually regeneration. In principle, XAS can be used for the analysis of speciation and evolution of Mo-species in Mo/ZSM-5 catalysts during all these stages. Taking all of the above into account, XAS is one of the most suitable tools for operando analysis of MDA catalysts. It should be noted that there are also several drawbacks to XAS analysis. Analysis of the structure of the active sites by extended X-ray absorption fine structure (EXAFS) analysis is difficult due to the bulk averaging nature of XAS. This is a particular problem for samples with a heterogeneous speciation, where active species and spectators may co-exist. XANES spectra can in principle be deconvoluted using spectra of reference compounds, while the latter are often based on bulk Mo references with long range order and less suitable for describing the highly dispersed Mo species inside zeolite pores. Therefore, complementary characterization techniques are often necessary to substantiate XAS findings for Mo/ZSM-5 catalysts during the MDA reaction.

One of the earliest XAS investigations of Mo/ZSM-5 was by Ding et al.,^[20] who studied the reduction and carburization of MoO_x in a 4 wt.% Mo/ZSM-5 catalyst by XANES, EXAFS, temper-

ature-programmed oxidation (TPO), and H/D exchange. The authors proposed that the initial Mo (VI)-oxo precursor is reduced and carburized to small MoC_x clusters (0.6–1 nm) upon exposure to CH_4 at 677°C . It was suggested that this process might result in a partial regeneration of the Brønsted acid sites that were initially occupied by MoO_x species. In a combined operando high energy resolution fluorescence detection X-ray absorption near edge spectroscopy (HERFD-XANES), X-ray emission spectroscopy (XES) and X-ray diffraction (XRD) study, Lezcano-González et al.^[21] followed the evolution of Mo-species in a 4 wt.% Mo/ZSM-5 catalyst during the MDA reaction at 677°C . The authors hypothesized that, during the reaction the initially dispersed Mo-oxo species were first converted into a metastable MoC_xO_y phase, and further partially detached from the framework to form MoC_3 centers. Furthermore, the Mo-containing species migrated out of the zeolite pores, and eventually formed Mo_2C agglomerates on the zeolite external surface. Using operando XANES, EXAFS, and high-resolution XRD, Agote-Arán et al.^[22] observed a significant detachment of Mo-species ($\sim 70\%$) in a 3.8 wt.% Mo/ZSM-5 catalyst. The authors proposed that these Mo-species migrated from the cation-exchange positions to the outer surface as $\text{Mo}_{1.6}\text{C}_3$ clusters during the MDA reaction at 700°C . In our recent work, using a combination of pulse reaction technique, operando XANES, EXAFS, and high-resolution high-angle annular dark-field scanning transmission electron microscopy (HAADF-STEM),^[23] we demonstrated that the dispersion of Mo-centers strongly depends on the Mo loading. While Mo-species in 1 wt.% Mo/ZSM-5 remained highly dispersed during the whole reaction, 5 wt.% Mo/ZSM-5 displayed a significant extent of Mo_2C formation on the external surface.

Previous XAS studies mainly focused on the induction period and early stages of the MDA reaction. The current work aims at providing a complete picture of the transformations of Mo-species in Mo/ZSM-5 catalysts during their whole lifetime, using in situ or operando XANES complemented by other characterization techniques. We focus on the following aspects: (i) the decomposition of the ammonium heptamolybdate precursor and the formation of dispersed Mo-oxo species; (ii) the evolution of Mo-species, the formation of carbon deposits inside zeolite pores and the nature of active Mo-sites during the activation and induction stages of the MDA reaction and (iii) the evolution of Mo-species during reductive/oxidative regeneration. The application of operando XANES combined with complementary techniques makes it possible to identify spectroscopic descriptors for the exchange process of MoO_x species on Brønsted acid sites, to obtain detailed insights into the structure and evolution of Mo-species and deposition of carbon inside the pores of working catalysts, and to determine the transformations of the used Mo/ZSM-5 catalysts upon regeneration in H_2 and O_2 flows.

Results and Discussion

Mo/ZSM-5 catalysts were prepared with a varying Mo loading (1–5 wt.%) by impregnation with ammonium heptamolybdate

tetrahydrate (AHM, $(\text{NH}_4)_6\text{Mo}_7\text{O}_{24}\cdot 4\text{H}_2\text{O}$). The stages of the molybdenum precursor decomposition, catalyst activation, MDA reaction and regeneration were investigated, using in situ or operando XANES, TG-MS, MCR-ALS analysis, operando XRD, pulse reaction technique, quasi in situ FTIR analysis of NO adsorption, and ^{27}Al MAS NMR.

Decomposition of AHM precursor

We first studied the process of AHM-impregnated catalyst precursor decomposition by TG-MS and in situ XANES. The mass loss during AHM decomposition was investigated by thermogravimetric analysis in the temperature range of 50–700 °C. As shown in Figure 1, the TG profiles feature three major decomposition steps, represented by peaks at 170, 420 and 670 °C in the DTG profiles. The total mass loss is in the 3.8–4.4 wt.% range. The data show that the first mass loss peak at 170 °C is nearly independent of the Mo loading and can be related to the removal of strongly adsorbed H_2O ($m/z=18$) from the zeolite pores (see MS data on Figure S1).^[24] The intensity of the second mass loss peak at 420 °C is proportional to the Mo loading, and signals of NO_x compounds ($m/z=30, 44$) derived from the oxidation of ammonium cations were observed in the MS spectra. Therefore, this region is related to the transformation of AHM into MoO_x on the zeolite external surface.^[25] Finally, a weaker broad third weight-loss feature proportional to the Mo content and accompanied by the formation of H_2O as the main product was observed from 550 to 700 °C. We assign this peak to the migration and exchange of Mo-oxo species with the Brønsted acid sites of zeolite.^[26] It is known that MoO_x species diffuse into the zeolite pores and react with the protons, resulting in the anchoring to the negatively charged framework Al centers as positively charged oxo-cations and leading to water formation. As demonstrated by Figure 1b, the exchange process of MoO_x within the zeolite channels is relatively slow (started around 550 °C), and likely diffusion-limited. Overall, the TG-MS results indicate that the decomposition of AHM precursor proceeds in three steps: (i) removal of adsorbed water, (ii) decomposition of AHM and (iii) slow exchange of mobile MoO_x species with Brønsted acid sites.

To derive spectroscopic descriptors for the formation of Mo-oxo species dispersed inside the zeolite pores, we performed an in situ XANES investigation of the process. For this purpose, the Mo K-edge XANES spectra were continuously recorded as a function of temperature and exposure time as displayed in Figure 2. First, the XANES spectra of 5% Mo/ZSM-5_IWI sample recorded between 50 and 170 °C are very similar (Figure 2a) and resemble the XANES spectrum of the AHM reference (Figure 2c). Thus, the local structure of the Mo-species is not significantly affected during the initial dehydration step. Then, an increasing intensity of the pre-edge feature (20.005 keV) was observed at 420 °C. This feature relates to the forbidden 1 s–4d electronic transition, which can take place in $[\text{MoO}_4]$ tetrahedra as well as in distorted $[\text{MoO}_6]$ octahedra due to p-d orbital mixing.^[27] It indicates the increasing contribution of Mo-species of tetrahedral symmetry and can be linked to the decomposition of AHM precursor. Upon increasing the temperature to 670 °C, the obtained spectrum resembles the Na_2MoO_4 reference, consisting exclusively of tetrahedral $[\text{MoO}_4]$ moieties. As the significant pre-edge feature is observed above 550 °C, we speculate that it is associated with the exchange of Mo-oxo species with zeolite Brønsted acid sites (i.e., the third step of AHM decomposition), leading to the high dispersion of MoO_x species inside the zeolite pores. It has been reported that these dispersed Mo-species anchored to zeolite framework are the precursors to the actual MDA active sites.^[23,28]

Differential in situ XANES (ΔXANES) at Mo K-edge enables straightforward monitoring of the structural changes during AHM decomposition.^[29] The ΔXANES spectra were obtained by subtraction of the first spectrum recorded at room temperature from all other spectra. As Figure 2b show, two main ΔXANES peaks are discerned at 20.005 and 20.023 keV. The evolution of the main ΔXANES features correlates with the DTG results in Figure 1b. As shown in Figure 2d, the increasing intensity of the 20.005 keV (pre-edge) feature points to the increasing concentration of tetrahedrally coordinated Mo-sites during the AHM decomposition process. This feature is also related to the increasing dispersion of MoO_x moieties. Several observations can be made by following the intensity of a negative ΔXANES feature at 20.023 keV. It represents the decreasing intensity of the first peak in the white line spectral region, which can be assigned to the loss of the long-range –Mo–O–Mo– order and

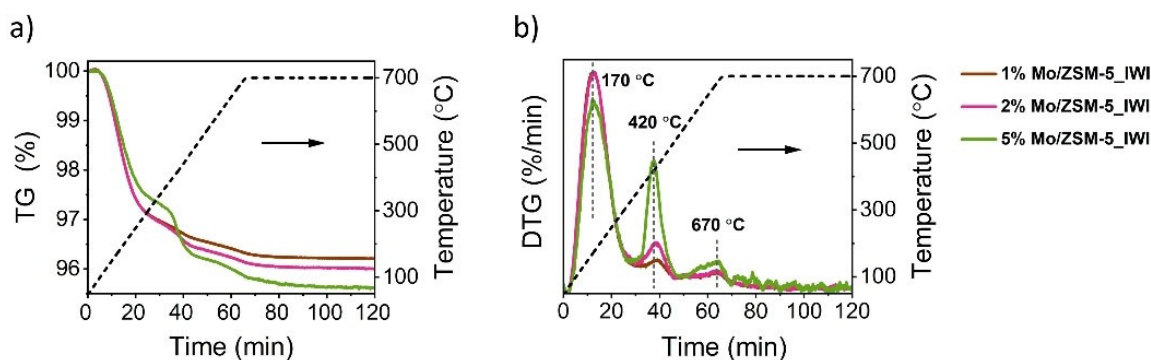


Figure 1. Thermal analysis profiles of as-impregnated AHM/ZSM-5 catalysts under air flow: (a) TG and (b) DTG profiles.

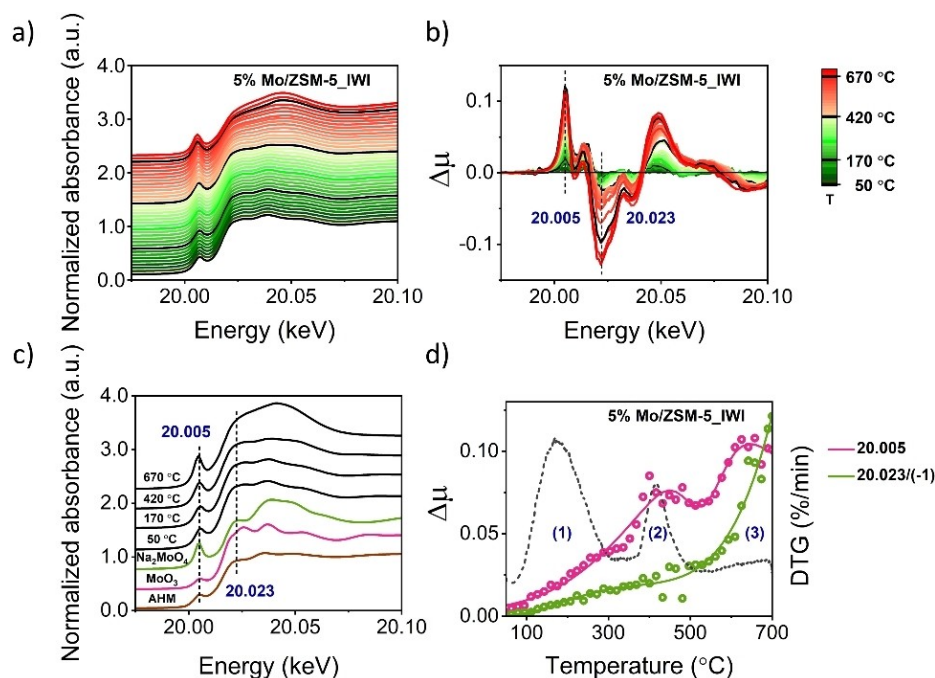


Figure 2. a) *In situ* Mo K-edge XANES spectra recorded during AHM precursor decomposition over 5% Mo/ZSM-5_IWI catalyst; b) corresponding Δ XANES spectra; c) comparison of XANES spectra obtained at typical temperature with three reference compounds and d) the intensity of the main Δ XANES feature together with DTG profile (dashed line) of 5% Mo/ZSM-5_IWI catalyst.

the formation of dispersed monomeric Mo-oxo species.^[30] From the sharp increase of the negative 20.023 keV feature above 550 °C (temperature for the third step of AHM decomposition), it can be inferred that it relates to the accelerated ion exchange process. Figure S2 shows that AHM precursor decomposition over the 2% Mo/ZSM-5_IWI sample also proceeds in three steps. The *in situ* spectra obtained for the low-loaded 1% Mo/ZSM-5_IWI sample recorded in transmission mode are not shown here, because they were too noisy to draw meaningful conclusions.

In line with TGA and Δ XANES data, principle component analysis (PCA) predicts three components for the recorded Mo K-edge spectra during AHM decomposition over 5% Mo/ZSM-5_IWI catalysts (Figures S3–6). Further, the multivariate curve resolution-alternating least squares (MCR-ALS) minimization was performed with three components, named hereafter W1, W2 and W3 (Figures 3a and S6b). The spectra of the pure components W1, W2 and W3 are similar to the experimental spectra obtained at 170, 420 and 670 °C (Figure 3a). The corresponding contribution of each component demonstrates that the formation of dispersed Mo-oxo centers starts at around 550 °C (Figure 3b).

In summary, *in situ* XANES combined with TG-MS can provide detailed insights into the evolution of the AHM precursor during its decomposition. Mo-species gradually evolve from an initial octahedral symmetry (AHM) to isolated tetrahedral Mo-oxo species via a MoO_x intermediate. The Δ XANES features at 20.005 and 20.023 keV are suitable descriptors for monitoring the decomposition of AHM precursor

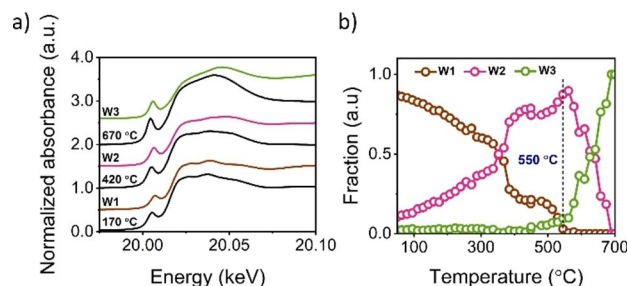


Figure 3. a) The spectra of the pure components (W1, W2 and W3) determined by MCR-ALS analysis from Mo K-edge XANES spectra, recorded during AHM precursor decomposition over 5% Mo/ZSM-5_IWI catalyst and b) corresponding contribution evolution profiles.

and exchange of the dispersed Mo-oxo species with the acid sites.

Next, the as-impregnated samples were calcined in air at 550 °C for a period of 8 h to ensure the completeness of AHM precursor decomposition. ICP results for these catalysts show that the obtained Mo loadings are comparable to the targeted values (Table S1). Based on XPS and XRD data (Figure S7) and our previous investigations,^[16b,23] the Mo-oxo species are dispersed inside the zeolite pores at Mo loading ≤ 2 wt.%, while 5% Mo/ZSM-5 contains a significant fraction of Mo-oxo agglomerates on the external surface. In this section, the evolution of Mo-species and carbon accumulation inside zeolite pores was monitored by operando XANES combined with MCR-ALS analysis and operando XRD. We focused on the 2% Mo/ZSM-5 catalyst, because the uniform Mo-species in 2% Mo/

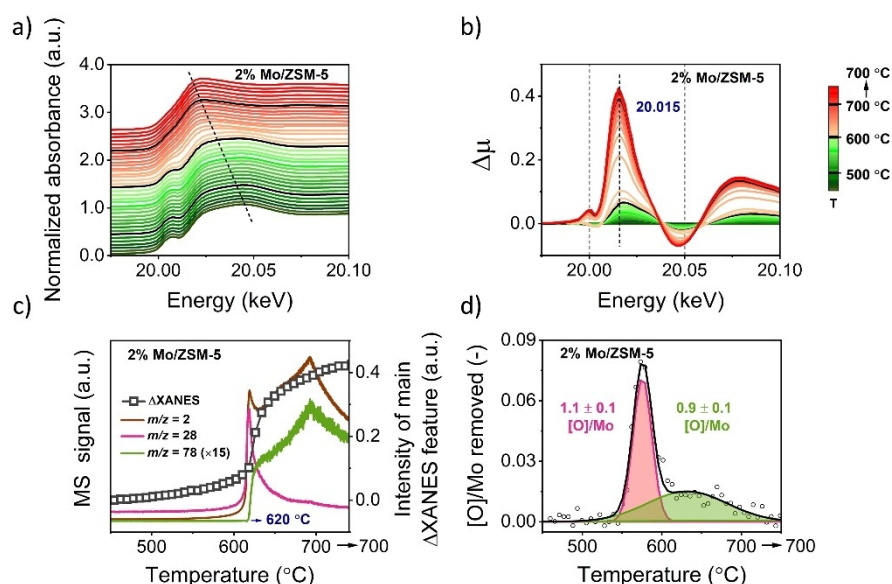


Figure 4. a) Operando Mo K-edge XANES spectra recorded during the MDA reaction over 2% Mo/ZSM-5 catalyst, in continuous CH_4 feed at 700 °C; b) corresponding $\Delta\mu$ spectra; c) Intensity of the MS signal together with main reduction ΔXANES feature at 20.015 keV and d) the ratio of removed [O]/Mo during the MDA reaction over 2% Mo/ZSM-5 catalyst derived from a separate CH_4 -TPR experiment.

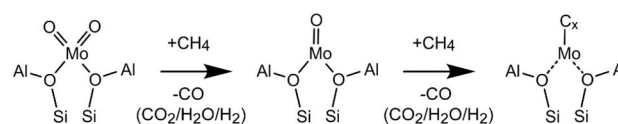
ZSM-5 catalyst are well-dispersed,^[16b,23] which make this sample optimal for operando XANES study and the interpretation of the XANES spectra by MCR-ALS analysis.

Evolution of Mo-species in continuous CH_4 feed

XANES spectra and relevant MS signals were recorded simultaneously during heating the catalyst to 700 °C in CH_4 flow. The position of Mo–K edge shifts to a lower energy (Figure 4a) with increasing temperature. In turn, the disappearing pre-edge feature can be linked to the reduction of Mo (VI).^[21,23] The evolution of Mo-species during the initial reaction stage was tracked by following the main ΔXANES reduction peak at 20.015 eV (Figure 4b). This peak corresponds to the shifting rising-edge feature. Product formation rates together with the intensity of this ΔXANES feature, are shown in Figure 4c as a function of temperature and exposure time.

Reduction of Mo-oxo species starts at 450 °C and continues even after 700 °C is reached, as evidenced by the increasing intensity of the 20.015 keV ΔXANES feature. The formation of benzene starts at 620 °C and increases until 700 °C. In the CH_4 flow, the removal of oxygen atoms from Mo-oxo species can be followed by measuring the formation of oxygen-containing products in the gas phase. The ratio of [O]/Mo derived from a separate CH_4 -TPR experiment (Figure 4d) indicates that the removal of oxygen atoms from Mo-centers proceeds in two steps. In both steps about one O atom per Mo atom is removed. The corresponding evolution of Mo-species during the CH_4 -TPR experiment is proposed in Scheme 1.

The two-step reduction process of Mo-species from 450 to 700 °C was further confirmed by PCA and MCR-ALS analysis. Three components can be used to fit the dataset (Figures S8–



Scheme 1. Proposed evolution of Mo-species during the initial stages of the MDA reaction.

11, 5a). The obtained spectra of the pure components, named C1, C2 and C3, were compared to that of the available references in Figure S11. The spectra of C1 is characterized by an intense pre-edge feature, which is similar to the Na_2MoO_4 reference with a tetrahedral symmetry of isolated Mo-centers. Pure components C2 and C3 cannot be readily identified on the basis of the measured references and spectra in literature.

Several observations can be made by analyzing the data in Figure 5b. First, the contribution of C1, corresponding to dispersed tetrahedral Mo(VI)-oxo species, decreases continu-

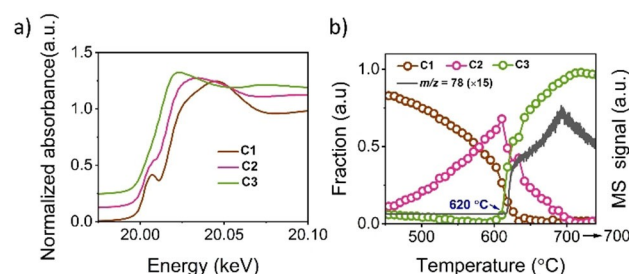


Figure 5. a) The spectra of the pure components (C1, C2 and C3) determined by MCR-ALS analysis from Mo K-edge XANES spectra, recorded over 2% Mo/ZSM-5 catalyst in continuous CH_4 feed and b) spectral component fraction profiles plotted together with $m/z = 78$ MS signal.

ously starting from 450 °C and completely disappears at 630 °C. Second, the contribution of an intermediate Mo-species, represented by C2, reaches a maximum contribution (70%) at 620 °C, followed by a rapid decrease until it is completely replaced by C3 at 700 °C. Based on the less intense pre-edge feature and the higher energy of the rising-edge feature as compared to MoO₂, C2 can be assigned to reduced Mo-oxo species with an oxidation state between 6+ and 4+ (Figure S11). We hypothesize that C2 corresponds to an intermediate Mo-oxo sites containing one oxygen atom (Scheme 1). C3 starts to form at about 620 °C, and its fraction further increases at the expense of C2. As the appearance of C3 coincides with the onset of benzene formation (Figure 5b), we assign this component to the main active species for the MDA reaction. These species are most likely related to a reduced dispersed Mo phase with contributions of Mo atoms in different oxidation states, ranging from 4+ to 0. Candidate phases include highly dispersed Mo-carbides or Mo-oxycarbides.

Accumulation of Coke Species in Continuous CH₄ Feed

Recently, we have shown that, in addition to the Mo-sites, surface carbon species play a catalytic role and are involved in the formation of benzene via a hydrocarbon pool-like mechanism.^[23,31] As hard X-ray absorption spectroscopy cannot be used to study hydrocarbons, we complemented the operando XANES study by an operando XRD investigation. This technique has been applied to study the evolution of the unit cell parameters of SAPO-34^[32] and ZSM-5^[33] catalysts during the methanol-to-hydrocarbons (MTH) reaction. Using operando synchrotron XRD, Rojo-Gama et al. demonstrated that the unit cell parameters (*a*-, *b*-, and *c*-unit cell vectors) of ZSM-5 catalyst vary depending on the amount and type of hydrocarbon molecules formed inside the zeolite pores. The authors proposed (*a*–*b*) parameter as a suitable descriptor of the catalyst deactivation and demonstrated that the difference between the *a*- and *b*-unit cell vectors is inversely proportional to the coke loading inside the pores.^[33]

Application of operando XRD in the MDA reaction is limited to the studies of Beale and co-workers. Lezcano-González et al. did not observe significant changes in XRD patterns of 4%Mo/ZSM-5 catalyst after 73.5 min of MDA reaction at 677 °C.^[21] The authors proposed that coke mainly accumulated on the external surface of zeolite crystals. Our previous results, however, provided evidence that coke and hydrocarbon pool molecules form inside the pores.^[31] To resolve this contradiction, we first performed ex situ powder XRD analysis of the fresh 2% Mo/ZSM-5 and the same catalyst after 16 h use in the MDA reaction at 700 °C (Figure S12). An expansion of the unit cell and a much lower difference between *a*- and *b*-unit cell vectors were observed for spent MDA catalysts (Table S2), in line with the results obtained for ZSM-5 catalysts after MTH reaction. These findings indicate that coke molecules are indeed formed inside the pores during the MDA reaction and, therefore, it should be possible to study their formation by operando XRD. Next, we monitored the evolution of the unit cell parameters at

700 °C at the beginning, middle and end of 2% Mo/ZSM-5 catalyst bed exposed to the flow of CH₄ (Figure 6a). XRD patterns were recorded during a 2.1 h operando experiment as shown in Figure 6b. The difference between the *a* and *b* unit cell vectors (*a*–*b*) (Figure 6c) steadily decreases during the whole experiment, indicating accumulation of hydrocarbon species inside the ZSM-5 pores. At the beginning of the reaction, the unit cell rapidly contracts (–0.15% of unit cell volume) followed by a slow expansion for longer time-on-stream (total increase of unit cell volume of ca. +0.25%) (Figure 6d). The rate of initial unit cell contraction and the extent of the final unit cell expansion are higher at the beginning of the bed than in the middle and, particularly, at the end of the bed (Figure 6d).

Comparison of the unit cell volume values and the intensity of the MS benzene signal (*m/z* = 78) demonstrate that the initial contraction of the unit cell coincides with the onset of benzene formation (Figure 7). The behavior of MFI unit cell upon adsorption of organic molecules is complicated and strongly

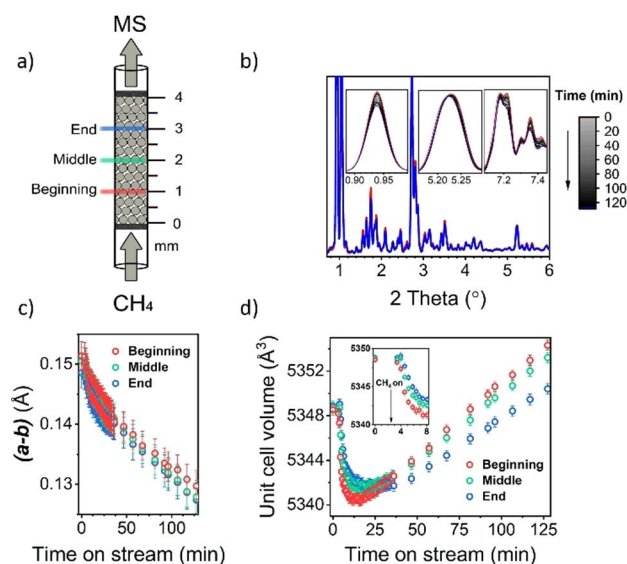


Figure 6. a) Positions within the catalyst bed where the XRD data were acquired; b) XRD patterns of 2%Mo/ZSM-5 catalyst recorded in the middle of the catalyst bed during 2.1 h of an operando experiment with methane was switched on at *t* = 150 s; c) difference of unit cell vectors *a* and *b*; d) Unit cell volumes derived from Rietveld refinement of operando XRD data.

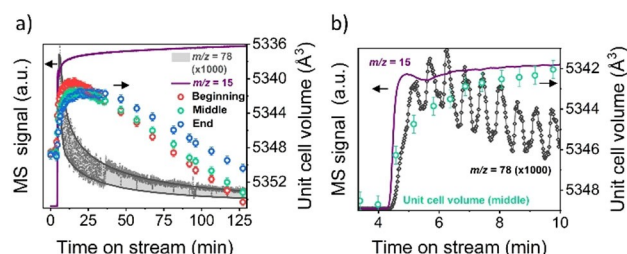


Figure 7. Comparison of unit cell volume recorded at three positions within the bed and MS signals *m/z* = 78 (benzene) and *m/z* = 15 (methane): a) whole experiment and b) first 10 min of the experiment.

depends on the type of adsorbate and its loading. It is known that adsorption of aromatic molecules in the intersections of ZSM-5 crystals leads to the contraction of the unit cell, while adsorption in the straight and sinusoidal channels results in expansion of the unit cell.^[34] We hypothesize that the initial contraction of the unit cell is related to the formation of hydrocarbon pool intermediates in the intersections of ZSM-5 crystals, while the slow expansion of the unit cell during prolonged reaction is related to the buildup of larger deactivating species in the straight and sinusoidal channels. To examine this hypothesis, we performed an in situ TG experiment with 2% Mo/ZSM-5 catalysts under similar reaction conditions and observed two stages of catalyst weight increase. At the beginning of the reaction (first 10–20 minutes), there is a rapid weight increase followed by a slower accumulation of coke for longer time on stream (Figure S14). The rapid stage can be linked to the initial contraction of the unit cell and formation of hydrocarbon pool species and the slow stage to deactivation. In this way, the higher extent of unit cell expansion upon deactivation corresponds to the higher coke loading at the beginning of the bed, as previously shown by Song et al.^[35] Finally, the faster contraction of the unit cell volume at the beginning of the catalyst bed can be rationalized by rapid accumulation of hydrocarbon pool components during catalyst induction. In the next session, we will focus on the evolution of Mo-species during the induction period.

Investigation of the nature of active Mo-sites

The fast transient processes occurring during the activation and induction stages of the MDA reaction complicate the characterization of active Mo-sites. Pulse reaction technique, where controlled doses of a reactant are periodically delivered to the reactor, allows titration of surface Mo-species of Mo/ZSM-5 catalysts during the MDA reaction.^[23,36] Furthermore, the structure of Mo-centers can be spectroscopically characterized at different reaction stages by, for example, quasi in situ FTIR spectroscopy with probe molecules. To verify that the pulsing of methane does not lead to severe concentration gradient within the catalyst bed in our experiments, we followed the evolution of Mo-species in the bottom, middle and top sections of the bed by operando XANES (Figures S15–16). The results evidence that the heterogeneities in the Mo speciation along the reactor bed are minor (Figure S16), and, thus, will not compromise the accuracy of the quasi in situ FTIR measurements. Next, catalyst samples were prepared by stopping the reaction after a certain number of pulses. For example, to obtain samples 1% Mo/ZSM-5_1 and 1% Mo/ZSM-5_10, pulsing of CH₄ over 1% Mo/ZSM-5 catalyst was stopped after 1 and 10 methane pulses after the onset of benzene formation, representing the beginning and the end of the induction stage respectively (Figure S17–18). The collected samples were transferred into an IR cell via a glovebox, and then the formed catalytic sites were characterized using quasi in situ FTIR analysis of NO adsorption.

The spectra of NO adsorbed on HZSM-5 and fresh Mo/ZSM-5 samples are similar, indicating that NO does not adsorb on the coordinatively saturated Mo (VI)-oxo species (Figure S19a). Three main bands were observed for all fresh samples. The band at 2133 cm⁻¹ can be attributed to NO⁺ exchanged on Brønsted acid sites, upon interaction with trace amounts of O₂.^[37] Physisorbed NO molecules on the zeolite gives rise to a band at 1877 cm⁻¹.^[38] The band at 1630 cm⁻¹ can be assigned to adsorbed water, formed during the exchange of Brønsted acid sites with NO⁺^[39] or bridged aluminum nitrate species.^[40]

After reduction of Mo/ZSM-5 by methane pulses, several new IR bands appear upon adsorption of NO (Figure 8). The most intensive bands at 1833 and 1731 cm⁻¹ can be assigned to, respectively, symmetric and asymmetric vibrations of dinitrosyl species adsorbed on reduced Mo-species.^[41] The intensities of these bands increase with the Mo loading and the number of CH₄ pulses, but their position remains the same. The 5% Mo/ZSM-5_10 sample yielded a noisy spectrum, which is due to the rapid initial carbon deposition during methane pulsing over this very active catalyst.

To underpin the assignment of the 1833 and 1731 cm⁻¹ bands to adsorbed dinitrosyls on reduced Mo-species, NO-FTIR spectra were recorded on reference samples consisting of 5 wt.% Mo on silica and alumina supports and treated with 20 pulses of methane at 700 °C (5% Mo/SiO₂_20 and 5% Mo/Al₂O₃_20, Figure S19b). As shown before, such treatment converts bulky Mo-oxo species into highly reduced supported Mo₂C nanoparticles with Mo in the formal oxidation state 2+.^[23] The FTIR spectra of adsorbed NO on these samples are dominated by dinitrosyl bands at 1708 and 1812 cm⁻¹ (Figure S19b). Comparable dinitrosyl bands were also observed on the zeolite-supported samples, although they are red-shifted for the two non-zeolite reference samples. As the NO stretching

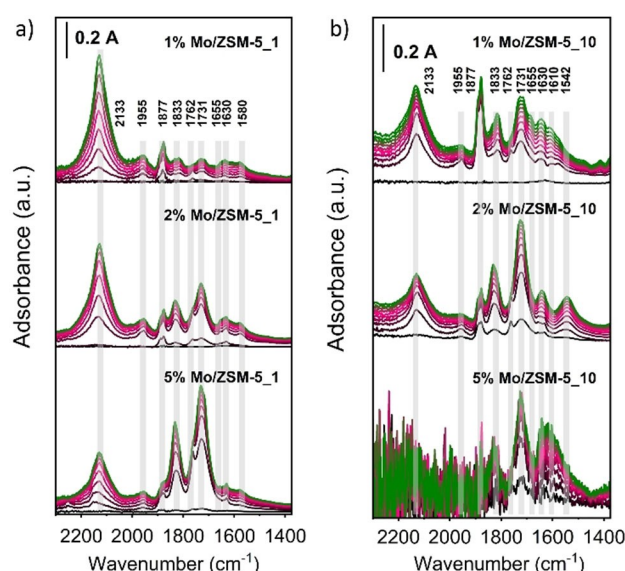


Figure 8. Evolution of the background-subtracted FTIR spectra of MDA catalyst samples: a) at the beginning and b) at the end of induction period upon exposure to 1 mbar pressure of nitric oxide. See Supporting Information for assignment of the observed bands (Table S3).

frequency in transition metal nitrosyls complexes usually increases with the oxidation state of the metal,^[38] the observed red shift suggests that the effective oxidation state of the Mo-species confined inside the zeolite pores is higher than 2+.

The spectra of reduced Mo/ZSM-5 samples also contain an intense single band at 1762 cm⁻¹, which slowly disappears with time in NO flow. This band is most likely related to a Mo⁵⁺-mononitrosyl, considering that Mo⁵⁺ can usually only coordinate one NO molecule.^[42] These Mo⁵⁺ species can be oxidized to Mo(VI)-species by NO during the FTIR measurements, which explains the disappearance of the 1762 cm⁻¹ band.^[43] In our previous work, the Mo⁵⁺ species were observed by electron paramagnetic resonance spectroscopy.^[23]

Overall, the obtained results indicate that Mo-sites formed on 1–5% Mo/ZSM-5 catalysts during activation and induction periods are of the same nature. These sites are reduced Mo-centers confined in the zeolite pores (different in nature from Mo₂C nanoparticles) with an effective oxidation state higher than 2+. The concentration of these species increases with the increasing Mo loading and extent of induction and, therefore, correlate to the catalytic activity.

Investigation of Mo-species and carbon deposits during reductive/oxidative regeneration

Coking deactivation of MDA catalysts appears inevitable, therefore, various regeneration strategies for Mo/ZSM-5 catalysts have been developed.^[16,44] Two main methods of regeneration can be distinguished: (i) combustion of coke in oxidative atmospheres and (ii) methanation of coke in H₂ flow. The stability of Mo/ZSM-5 catalysts during reaction-regeneration processes is an important aspect and it is closely related to the structure of Mo-oxo species.^[16] We applied operando XANES-MS, TGA, ²⁷Al MAS NMR, and XRD to monitor the evolution of Mo-species and coke deposits in the 2% and 5% Mo/ZSM-5 catalysts during reductive and oxidative regeneration processes at 700 °C.

The 2% and 5% Mo/ZSM-5 catalysts were first exposed to CH₄ flow for 1 h at 700 °C. During this treatment reduced active Mo-species were formed, as confirmed by the disappearing of pre-edge feature, shifting of Mo K-edge to lower energy, and high rate of benzene formation (Figure 9). The benzene (*m/z* = 78) yield reaches a maximum after 20 min of the MDA reaction, followed by a gradual decrease due to deactivation (Figures 9b and 9d). Reductive regeneration of the partially deactivated catalysts in H₂ flow was performed. A sharp methane (*m/z* = 15) signal appeared directly after switching to H₂ flow (Figures 9b and 9d). The methanation of coke is indicative of the reversible nature of MDA coke formation.^[45] No significant difference between the XANES spectra recorded before and after H₂ regeneration was observed (Figures 9a and 9c). This finding indicates that regeneration at 700 °C under reductive conditions does not lead to structural changes in Mo-species. The removal of coke species by H₂ treatment is incomplete, as only 33% and 56% of carbon deposits has been eliminated from coked 2% and 5% Mo/ZSM-5 (Table 1).

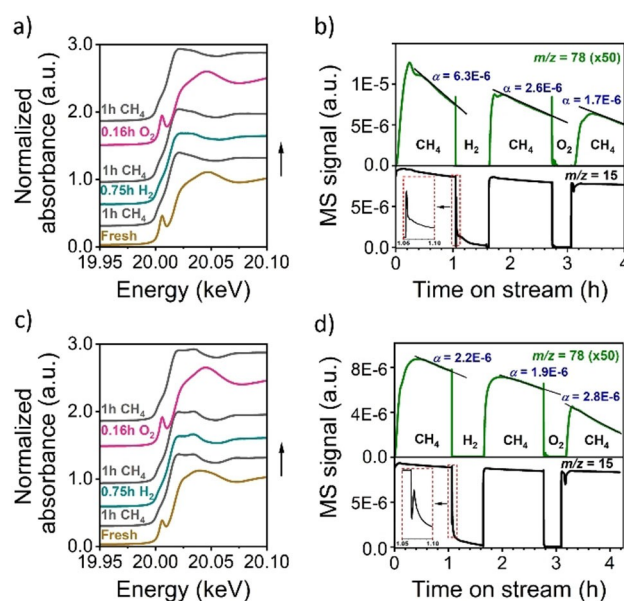


Figure 9. Operando Mo K-edge XANES spectra: a) 2% Mo/ZSM-5 and c) 5% Mo/ZSM-5 catalyst. Corresponding MS intensity of *m/z* = 15 and 78: b) 2% Mo/ZSM-5 and d) 5% Mo/ZSM-5 catalyst recorded during reaction-regeneration processes.

| Sample | 1 h CH ₄ [mg/g _{cat}] | 0.75 h H ₂ [mg/g _{cat}] | 0.16 h O ₂ [mg/g _{cat}] |
|-------------|---|---|---|
| 2% Mo/ZSM-5 | 26.17 | 17.50 (−33%) | 1.60 (−94%) |
| 5% Mo/ZSM-5 | 24.48 | 10.82 (−56%) | 1.00 (−96%) |

Next, the H₂-treated catalysts underwent a second reaction stage by switching back to CH₄ flow. An increase in benzene (*m/z* = 78) MS signal indicates that the catalytic activity is recovered after reductive regeneration (Figures 9b and 9d). Upon coke combustion in O₂ flow, the pre-edge feature appears and the Mo–K edge shifts to a higher energy, indicating oxidative oxidation of Mo-sites back to 6+ oxidation state. Based on TGA results, more than 90% of the coke species have been removed from both catalysts. The benzene (*m/z* = 78) formation in the final reaction stage over 2% Mo/ZSM-5 catalyst slightly increases after regeneration in O₂, but it dramatically decreases for the 5% Mo/ZSM-5 catalyst, and a higher deactivation rate constant was observed for this catalyst (Figures 9b and 9d). Clearly, the stability of Mo/ZSM-5 catalysts during isothermal oxidative regeneration strongly depends on the Mo loading.^[16b]

The catalyst samples obtained after reaction and regeneration stages were analyzed by ²⁷Al MAS NMR and XRD. First, the dominant signals at 53 ppm and 0 ppm in ²⁷Al NMR spectra of the 2% and 5% Mo/ZSM-5 catalysts can be ascribed to framework and extra framework aluminum species with respectively tetrahedral and octahedral coordination (Figures 10a and 10b). The difference between the spectra of the coked catalyst and H₂-treated catalysts is small, confirming that H₂ regeneration does not substantially affect the zeolite

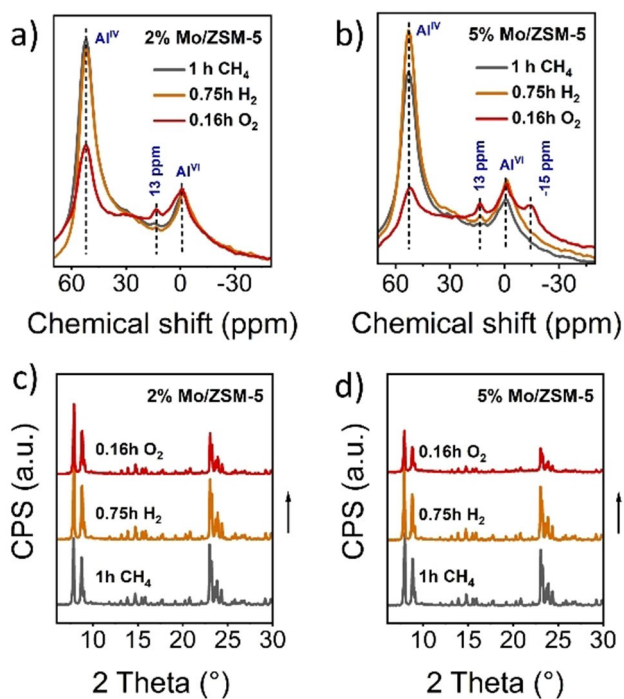


Figure 10. a, b) ^{27}Al MAS NMR spectra and c, d) XRD patterns at 2 theta of 7° – 10° for 2% and 5% Mo/ZSM-5 catalysts.

structure. However, after regeneration in O_2 , the framework Al signal at 53 ppm is broadened and reduced in intensity, indicating the extensive dealumination of the zeolite framework.^[46] Two new signals at around 13 ppm and -15 ppm appeared, in particular for the O_2 -treated 5% Mo/ZSM-5 catalyst, due to the formation of $\text{Al}_2(\text{MoO}_4)_3$ phase.^[6c,47] This process is accompanied by a partial loss of crystallinity evidenced by XRD analysis, where the 5% Mo/ZSM-5 catalyst obtained after O_2 treatment shows the most substantial decrease of crystallinity.

To summarize, compared to oxidative regeneration where coke can be efficiently removed, reductive regeneration at 700°C is less effective. However, methanation of coke in H_2 flow is still promising, considering that it does not lead to the oxidation of active Mo-centers, reaction of Mo-oxo species with framework Al and consequent degradation of the zeolite structure.

Conclusion

We demonstrate that in situ/operando XANES combined with complementary tools is a powerful method to study the evolution of Mo/HZSM-5 from the preparation of Mo-oxo precursors to the regeneration of used catalysts. XANES is especially useful for zeolite-based catalysts, where the active sites are well-dispersed within catalyst bulk and often inaccessible for surface-sensitive techniques. We distinguished three steps of AHM precursor decomposition by in situ XANES combined with TG-MS. AHM precursor is first dehydrated, and

with increasing temperature, the Mo-oxo evolved into highly dispersed tetrahedral $[\text{MoO}_4]$ species. Diffusion-limited exchange of these species with Brønsted acid sites inside the zeolite pores occurs at temperatures $>550^\circ\text{C}$. We derived spectroscopic ΔXANES descriptors for the AHM decomposition and exchange of Mo-oxo species with the acid sites. The two-step reduction process of Mo-species during the reaction in methane flow was observed by CH_4 -TPR and MCR-ALS analysis of operando XANES data. The accumulation of coke species within the ZSM-5 pores was monitored by operando XRD. The initial contraction of the unit cell coincides with benzene formation and it is related to the formation of hydrocarbon pool intermediates. The unit cell expands upon catalyst deactivation and we linked this behavior to the accumulation of deactivating coke species. Furthermore, a combination of pulse reaction technique with operando XANES and quasi in situ FTIR analysis of NO adsorption was employed to study the structure of Mo-sites during the catalyst activation. The results show that the active sites in all studied Mo/ZSM-5 catalysts are similar, regardless of the Mo content. Finally, isothermal reductive and oxidative regeneration procedures were monitored by operando XANES-MS, ^{27}Al MAS NMR and ex situ XRD. Although oxidative regeneration leads to almost complete removal of carbon, it can be destructive for the zeolite structure due to the re-oxidation of Mo-sites to reactive Mo-oxo species accompanied by the formation of $\text{Al}_2(\text{MoO}_4)_3$. This process is especially pronounced at higher molybdenum loading. Reductive regeneration with H_2 resulted in incomplete removal of coke via methanation, but it is favorable for preserving the catalyst structure.

Experimental Section

Catalyst preparation

Ammonium heptamolybdate tetrahydrate (AHM, $(\text{NH}_4)_6\text{Mo}_7\text{O}_{24}\cdot 4\text{H}_2\text{O}$) was purchased from Merck and used without further purification. Supported Mo catalysts were prepared by incipient wetness impregnation of commercial HZSM-5 zeolite powder ($\text{Si}/\text{Al}=13$, Süd-Chemie, now Clariant) with an aqueous solution of AHM of desirable concentration. After impregnation, the catalysts were dried at 110°C overnight. Depending on the Mo loading, the as-impregnated samples were denoted as x% Mo/ZSM-5_IWI, where x represents the Mo weight loading (1, 2 or 5 wt.%). The as-impregnated samples were further calcined in air at 550°C for 8 h, with a ramp rate of 2°C min^{-1} . The calcined samples were denoted as x% Mo/ZSM-5, where x is the Mo weight loading. Reference 5% Mo/ SiO_2 and 5% Mo/ Al_2O_3 materials were prepared using the same method.

Catalyst characterization

Operando X-ray Absorption Spectroscopy. X-ray Absorption Near Edge Structure (XANES) spectra were collected at the Mo K-edge (20.0 keV) in transmission mode at the BM26 A (DUBBLE) beamline^[48] of the European Synchrotron Radiation Facility, Grenoble, France. The energy was selected with a Si (111) monochromator and calibrated with molybdenum foil ($E_0=20.0$ keV). For the operando measurements, a home-built fixed-bed reactor was used.

The catalyst sample in the form of fine pellets (75–125 μm) was placed inside quartz tubes (length 250 mm, i.d. 4 mm, o.d. 5 mm) with a flattened section in the middle (length 20 mm, thickness of about 0.25 mm) to improve the transmission signal as discussed in detail elsewhere.^[23] The recorded XANES spectra were normalized with Athena software (Demeter v.0.9.26).^[49]

Multivariate Curve Resolution (MCR) Analysis. XANES spectra were analyzed by the combination of Principal Component Analysis (PCA) and Multivariate Curve Resolution with Alternating Least Squares (MCR-ALS). The number of pure components characterizing the normalized XANES datasets was determined by PCA analysis, using a Singular Value Decomposition (SVD) algorithm. MCR-ALS analysis was performed with the MAX (Multiplatform Applications for XAFS) software package.^[50] Non-negative constraints were applied to the pure component spectra and their fractions, and the cumulative contribution profile closure was set to unity. The convergence criterion for the MCR-ALS analysis was a standard deviation of the residuals lower than or equal to 0.1% between two consecutive iterations. Detailed description of the MCR-ALS application to XAS can be found in several recent studies.^[51]

Operando Powder X-ray Diffraction (XRD). Operando XRD experiments were performed at the ID31 beamline (ESRF, DOI: 10.15151/ESRF-ES-432202550). The photon wavelength was 0.018233 nm (68 keV) with a focused beam of 0.5 mm \times 0.5 mm, and a Pilatus3 X CdTe 2 M X-ray detector (Dectris) was used. Sieved (125–250 μm) Mo/ZSM-5 catalyst (15 mg) was placed in a quartz capillary (i.d. 2.8 mm, o.d. 3.0 mm, wall thickness 0.1 mm) to form a catalyst bed of 4 mm in length. The capillary was sealed by PTFE ferrules in a home-built Clausen-type flow cell,^[52] located on a movable sample stage. The catalyst bed was heated to 700 °C using two gas blowers (Cyberstar). The temperature was controlled by a thin (0.25 mm) K-type thermocouple placed inside the catalyst bed. The catalyst was exposed to a flow of CH₄ (18 mL/min) and Ar (2 mL/min). The chemical composition of the outlet flow was analyzed by a quadrupole mass-spectrometer (OmniStar, Balzers). The capillary was moved up and down during the experiment to acquire diffractograms at different positions of the bed. The integrated XRD patterns were analyzed by Rietveld refinement using the GSAS-II software. The patterns were refined in the 2-theta region of 0.6–9.35 °. The scale factor, background, and the unit cell parameters (*Pnma* space group) were refined. Other parameters (crystal size, strain, displacement, atomic and thermal parameters, etc.) were kept the same for each pattern.

Fourier Transform Infrared Spectroscopy (FTIR) Analysis of Nitrogen Monoxide (NO) Adsorption. Quasi in situ NO adsorption experiments followed by transmission FTIR were performed using a Bruker ALPHA FTIR spectrometer and a home-built environmental cell, both placed inside a glovebox (O₂ level < 1 ppm and H₂O level < 2 ppm). The sample in a form of a self-supporting wafer (diameter 1.3 cm, weight 10–15 mg), contained between two calcium fluoride (CaF₂) windows, was placed in the cell. During FTIR measurements, a continuous diluted flow of NO (1 mbar in He) was maintained. Prior to the measurements, the catalyst samples were exposed to a certain number of 5 mL CH₄ pulses at 700 °C and then transferred to the glovebox without exposure to air.

X-ray Photoelectron Spectroscopy (XPS). The concentration of Mo-species on the surface of catalysts was determined by XPS with a Thermo Scientific K-alpha spectrometer, equipped with a monochromatic Al K α (1486.6 eV, 72 W) X-ray source, and a 180° double-focusing hemispherical analyzer with a 128-channel detector. The spectrometer was operated at a vacuum higher than 10⁻⁸ mbar, a spot size of 400 μm and pass energy of 200 eV. XPS spectra of the Al 1s, Si 2p and Mo 3d core lines were recorded. All binding energies (BE) were calibrated using the C 1s binding energy of

adventitious carbon (C 1s = 284.8 eV). Spectra were analyzed with the CasaXPS software (version 2.3.23). Quantification of the surface concentration of the relevant elements was done using atomic sensitivity factors.^[53]

Inductively Coupled Plasma Optical Emission Spectroscopy (ICP-OES). The actual Mo content was analyzed using ICP-OES (Spectro CIROS CCD) spectrometer. Prior to analysis, the samples were dissolved in 1:1:1 (by weight) mixture of HF (40%): HNO₃ (60%): H₂O.

²⁷Al Magic-Angle Spinning Nuclear Magnetic Resonance (MAS NMR). NMR spectra were recorded at room temperature with 11.7 T Bruker DMX500 NMR spectrometer. The measurements were carried out at 132 MHz with a spinning rate of 25 kHz and a single citation pulse length of 1 μs with 1 s repetition time. Chemical shift were referenced to an saturated Al(NO₃)₃ solution.

Thermogravimetric analysis (TGA) of spent samples. Mettler Toledo TGA/DSC 1 instrument was applied for the coke content determination of Mo/ZSM-5 sample. About 30 mg of a catalyst sample was placed in an alumina crucible. The uncovered crucible was heated up to 800 °C at a rate of 5 °C min⁻¹ in 40 mL/min He + 20 mL/min O₂ flow.

X-ray Diffraction (XRD). *Ex situ* XRD patterns were obtained with a Bruker D2 powder diffractometer using Cu K α radiation (scan speed 0.01 °/s, 2 theta range from 5 to 60°).

Catalytic testing

AHM Precursor Decomposition. The decomposition of zeolite-supported AHM under air flow was followed with a thermogravimetric analyzer (TG, Discovery HP TGA 75, TA Instruments) coupled with a mass spectrometer (MS, GeneSys, ESS). About 30 mg of as-impregnated sample was heated in an uncovered alumina crucible from 50 to 700 °C at a rate of 10 °C /min, followed by an isothermal dwell of 1 h at 700 °C. The evolved gases were analyzed by a mass spectrometer using *m/z* = 17, 18, 30, and 44, respectively for NH₃ or OH, H₂O, NO, and N₂O. Background data were obtained by applying the same treatment to the used sample after cooling to ambient temperature.

MDA Reaction in Continuous and Pulsed Modes. Methane aromatization in continuous CH₄ feed was carried out in a setup described in detail before.^[38] The quartz reactor (i.d. 4.0 mm, length 250 mm) was sealed with Viton® O-rings. The temperature of the home-built oven was controlled by a calibrated thermocouple and a Eurotherm temperature controller, while the gases were supplied using calibrated mass flow controllers (Brooks). The reactor effluent was analyzed by online mass spectrometry (Pfeiffer Omnistar GSD 301 T3 spectrometer).

An amount of 500 mg of sieved catalyst (125–250 μm) was placed between two quartz wool plugs inside the isothermal (700 °C) zone of the oven. In continuous CH₄ feed mode, reactions were performed in a flow that consisted of 10 mL/min CH₄ and 20 mL/min He. In order to remove organic residues and water, the catalysts were heated from room temperature to 450 °C at a rate of 5 °C min⁻¹, followed by an isothermal dwell of 45 min. Then the temperature was increased to 700 °C at a rate of 2 °C min⁻¹ afterwards. In pulse CH₄ mode, the same temperature program was followed under 30 mL/min Ar flow. Once 700 °C was reached, short CH₄ pulses were delivered into Ar flow every 200 sec, by an automated 6-way valve equipped with a 5 mL sample loop. XANES spectra were recorded at the same time for both continuous/pulsed CH₄ feed modes. During the operando pulse study, XANES spectra were taken after each two methane pulses.

Temperature-Programmed Reduction in Continuous CH₄ feed (CH₄-TPR). To discriminate the MoO_x reduction stages, a CH₄-TPR experiment was conducted. An amount of 500 mg of sieved catalyst (125–250 μm) was placed in the reactor and heated from room temperature to 700 °C (isothermal dwell at 700 °C of 30 min) at a slow ramp rate of 2 °C min⁻¹ in a mixed flow of 15 mL/min CH₄ and 30 mL/min He. The total number of oxygen atoms removed was accurately quantified from integration of CO₂, H₂O and CO peaks derived from online gas chromatography (Interscience Compact GC). Results of three identical experiments were averaged to obtain the final CH₄-TPR profile.

Regeneration in O₂ and H₂ flow. Regeneration experiments were performed using the same setup. First, Mo/ZSM-5 samples were exposed to CH₄ flow of 15 mL/min for 1 h at 700 °C. The partially deactivated catalysts were regenerated in a H₂ flow of 15 mL/min for 45 min (0.75 h). After the first regeneration step, the activated catalysts were exposed to CH₄ feed again followed by a second reaction stage. Then, an oxidative regeneration of the catalyst for 10 min (0.16 h), under flow of O₂ of 15 mL/min at 700 °C was performed. Finally, the catalytic test in CH₄ feed was repeated for the third time. XANES spectra and MS signals were recorded continuously during the whole procedure. We estimated the deactivation rates (α) of the catalysts by linear fitting the slope of benzene signal.

Acknowledgements

Financial support from China Scholarship Council (201806930028) is gratefully acknowledged. We acknowledge the European Synchrotron Radiation Facility for provision of synchrotron radiation facilities and we would like to thank Jacob Drnec for assistance in using beamline ID31.

Conflict of Interest

The authors declare no conflict of interest.

Data Availability Statement

The data that support the findings of this study are available from the corresponding author upon reasonable request.

Keywords: Methane dehydroaromatization · Mo/ZSM-5 · Operando XANES · Pulse reaction · Regeneration

- [1] a) A. I. Olivos-Suarez, Á. Szécsényi, E. J. M. Hensen, J. Ruiz-Martinez, E. A. Pidko, J. Gascon, *ACS Catal.* **2016**, *6*, 2965–2981; b) E. V. Kondratenko, T. Poppel, D. Seeburg, V. A. Kondratenko, N. Kalevaru, A. Martin, S. Wohlrab, *Catal. Sci. Technol.* **2017**, *7*, 366–381; c) J. N. Armor, *J. Energy Chem.* **2013**, *22*, 21–26.
- [2] J. A. Labinger, J. E. Bercaw, *Nature* **2002**, *417*, 507–514.
- [3] a) E. McFarland, *Science* **2012**, *338*, 341–342; b) V. L. Sushkevich, D. Palagin, M. Ranocchiari, J. A. Van Bokhoven, *Science* **2018**, *359*, 523–527; c) P. Tang, Q. Zhu, Z. Wu, D. Ma, *Energy Environ. Sci.* **2014**, *7*, 2580–2591; d) X. Guo, G. Fang, G. Li, H. Ma, H. Fan, L. Yu, C. Ma, X. Wu, D. Deng, M. Wei, D. Tan, R. Si, S. Zhang, J. Li, L. Sun, Z. Tang, X. Pan, X. Bao, *Science* **2014**, *344*, 616–619; e) D. C. Upham, V. Agarwal, A. Khechfe, Z. R. Snodgrass, M. J. Gordon, H. Metiu, E. W. McFarland, *Science* **2017**, *358*, 917–921.

- [4] a) Z. R. Ismagilov, E. V. Matus, L. T. Tsikoza, *Energy Environ. Sci.* **2008**, *1*, 526–541; b) J. J. Spivey, G. Hutchings, *Chem. Soc. Rev.* **2014**, *43*, 792–803.
- [5] a) C. Zhang, S. Li, Y. Yuan, W. Zhang, T. Wu, L. Lin, *Catal. Lett.* **1998**, *56*, 207–213; b) S. Ma, X. Guo, L. Zhao, S. Scott, X. Bao, *J. Energy Chem.* **2013**, *22*, 1–20; c) N. A. Mamonov, E. V. Fadeeva, D. A. Grigoriev, M. N. Mikhailov, L. M. Kustov, S. A. Alkhimov, *Russ. Chem. Rev.* **2013**, *82*, 567–585.
- [6] a) N. Kosinov, F. J. A. G. Coumans, E. Uslamin, F. Kapteijn, E. J. M. Hensen, *Angew. Chem. Int. Ed.* **2016**, *55*, 15086–15090; *Angew. Chem.* **2016**, *128*, 15310–15314; b) N. Kosinov, E. J. M. Hensen, *Adv. Mater.* **2020**, 2002565; c) C. H. L. Tempelman, E. J. M. Hensen, *Appl. Catal. B* **2015**, 176–177, 731–739.
- [7] H. Liu, W. Shen, X. Bao, Y. Xu, *J. Mol. Catal. A* **2006**, *244*, 229–236.
- [8] E. V. Matus, I. Z. Ismagilov, O. B. Sukhova, V. I. Zaikovskii, L. T. Tsikoza, Z. R. Ismagilov, J. A. Moulijn, *Ind. Eng. Chem. Res.* **2007**, *46*, 4063–4074.
- [9] H. Zheng, D. Ma, X. Bao, Z. H. Jian, H. K. Ja, Y. Wang, C. H. F. Peden, *J. Am. Chem. Soc.* **2008**, *130*, 3722–3723.
- [10] I. Vollmer, N. Kosinov, Á. Szécsényi, G. Li, I. Yarulina, E. Abou-Hamad, A. Gurinov, S. Ould-Chikh, A. Aguilar-Tapia, J. L. Hazemann, E. Pidko, E. Hensen, F. Kapteijn, J. Gascon, *J. Catal.* **2019**, *370*, 321–331.
- [11] M. T. Portilla, F. J. Llopis, C. Martínez, *Catal. Sci. Technol.* **2015**, *5*, 3806–3821.
- [12] Y. Song, Q. Zhang, Y. Xu, Y. Zhang, K. Matsuoka, Z. G. Zhang, *Appl. Catal. A* **2017**, *530*, 12–20.
- [13] J. Bedard, D.-Y. Hong, A. Bhan, *J. Catal.* **2013**, *306*, 58–67.
- [14] P. L. Tan, Y. L. Leung, S. Y. Lai, C. T. Au, *Catal. Lett.* **2002**, *78*, 251–258.
- [15] Z. Liu, M. A. Nutt, E. Iglesia, *Catal. Lett.* **2002**, *81*, 271–279.
- [16] a) J. Gao, Y. Zheng, J. M. Jehng, Y. Tang, I. E. Wachs, S. G. Podkolzin, *Science* **2015**, *348*, 686–690; b) N. Kosinov, F. J. A. G. Coumans, G. Li, E. Uslamin, B. Mezari, A. S. G. Wijkema, E. A. Pidko, E. J. M. Hensen, *J. Catal.* **2017**, *346*, 125–133; c) S. J. Han, S. K. Kim, A. Hwang, S. Kim, D. Y. Hong, G. Kwak, K. W. Jun, Y. T. Kim, *Appl. Catal. B* **2019**, *241*, 305–318.
- [17] a) J. Singh, C. Lamberti, J. A. van Bokhoven, *Chem. Soc. Rev.* **2010**, *39*, 4754–4766; b) I. Vollmer, S. Ould-Chikh, A. Aguilar-Tapia, G. Li, E. Pidko, J. L. Hazemann, F. Kapteijn, J. Gascon, *J. Am. Chem. Soc.* **2019**, *141*, 18814–18824.
- [18] D. I. Sharapa, D. E. Doronkin, F. Studt, J.-D. Grunwaldt, S. Behrens, *Adv. Mater.* **2019**, *31*, 1–12.
- [19] a) M. Wakizaka, A. Atqa, W.-J. Chun, T. Imaoka, K. Yamamoto, *Nanoscale* **2020**, *12*, 15814–15822; b) J. Zhu, E. A. Uslamin, N. Kosinov, E. J. M. Hensen, *Catal. Sci. Technol.* **2020**, *10*, 3635–3645.
- [20] W. Ding, S. Li, G. D. Meitzner, E. Iglesia, *J. Phys. Chem. B* **2001**, *105*, 506–513.
- [21] I. Lezcano-González, R. Oord, M. Rovezzi, P. Glatzel, S. W. Botchway, B. M. Weckhuysen, A. M. Beale, *Angew. Chem. Int. Ed.* **2016**, *55*, 5215–5219; *Angew. Chem.* **2016**, *128*, 5301–5305.
- [22] M. Agote-Arán, A. B. Kroner, H. U. Islam, W. A. Stawirski, D. S. Wragg, I. Lezcano-González, A. M. Beale, *ChemCatChem* **2019**, *11*, 473–480.
- [23] N. Kosinov, A. S. G. Wijkema, E. Uslamin, R. Rohling, F. J. A. G. Coumans, B. Mezari, A. Parastaev, A. S. Poryvaev, M. V. Fedin, E. A. Pidko, E. J. M. Hensen, *Angew. Chem. Int. Ed.* **2018**, *57*, 1016–1020; *Angew. Chem.* **2018**, *130*, 1028–1032.
- [24] a) F. Ayari, E. Mannei, E. Asedegbega-Nieto, M. Mhamdi, A. R. Guerrero-Ruiz, G. Delahay, A. Ghorbel, *J. Therm. Anal. Calorim.* **2018**, *131*, 1295–1306; b) F. Ayari, E. Mannei, E. Asedegbega-Nieto, M. Mhamdi, A. R. Guerrero-Ruiz, G. Delahay, A. Ghorbel, *React. Kinet. Mech. Catal.* **2018**, *124*, 419–436.
- [25] a) A. Chithambararaj, D. B. Mathi, N. R. Yogamalar, A. C. Bose, *Mater. Res. Express* **2015**, *2*, 055004; b) R. Murugan, H. Chang, *J. Chem. Soc. Dalton Trans.* **2001**, 3125–3132; c) W. M. Shaheen, *Mater. Sci. Eng. A* **2007**, *445*–446, 113–121.
- [26] a) H. Liu, W. Shen, X. Bao, Y. Xu, *Appl. Catal. A* **2005**, *295*, 79–88; b) W. Li, G. D. Meitzner, R. W. Borry, E. Iglesia, *J. Catal.* **2000**, *191*, 373–383; c) R. W. Borry, Y. H. Kim, A. Huffsmith, J. A. Reimer, E. Iglesia, *J. Phys. Chem. B* **1999**, *103*, 5787–5796.
- [27] a) H. Wen, B. M. Cheng, P. A. Tanner, *RSC Adv.* **2017**, *7*, 26411–26419; b) S. E. Shadle, B. Hedman, K. Hodgson, E. I. Solomon, *Inorg. Chem.* **1994**, *33*, 4235–4244.
- [28] I. Vollmer, G. Li, I. Yarulina, N. Kosinov, E. J. Hensen, K. Houben, D. Mance, M. Baldus, J. Gascon, F. Kapteijn, *Catal. Sci. Technol.* **2018**, *8*, 916–922.
- [29] a) D. E. Ramaker, D. C. Koningsberger, *Phys. Chem. Chem. Phys.* **2010**, *12*, 5514–5534; b) A. L. Bugaev, A. A. Guda, A. Lazzarini, K. A. Lomachenko, E. Groppo, R. Pellegriani, A. Piovano, H. Emerich, A. V. Soldatov, L. A.

- Bugaev, V. P. Dmitriev, J. A. van Bokhoven, C. Lamberti, *Catal. Today* **2017**, *283*, 119–126.
- [30] M. Agote-Arán, R. E. Fletcher, M. Briceno, A. B. Kroner, I. V. Sazanovich, B. Slater, M. E. Rivas, A. W. J. Smith, P. Collier, I. Lezcano-González, A. M. Beale, *ChemCatChem* **2020**, *12*, 294–304.
- [31] N. Kosinov, E. A. Uslamin, F. J. A. G. Coumans, A. S. G. Wijkema, R. Y. Rohling, E. J. M. Hensen, *ACS Catal.* **2018**, *8*, 8459–8467.
- [32] a) D. S. Wragg, R. E. Johnsen, M. Balasundaram, P. Norby, H. Fjellvåg, A. Grønvdal, T. Fuglerud, J. Hafizovic, Ø. B. Vistad, D. Akporiaye, *J. Catal.* **2009**, *268*, 290–296; b) D. S. Wragg, M. G. O'Brien, F. L. Bleken, M. Di Michiel, U. Olsbye, H. Fjellvåg, *Angew. Chem. Int. Ed.* **2012**, *51*, 7956–7959; *Angew. Chem.* **2012**, *124*, 8080–8083.
- [33] a) D. Rojo-Gama, M. Nielsen, D. S. Wragg, M. Dyballa, J. Holzinger, H. Falsig, L. F. Lundegaard, P. Beato, R. Y. Brogaard, K. P. Lillerud, U. Olsbye, S. Svelle, *ACS Catal.* **2017**, *7*, 8235–8246; b) D. Rojo-Gama, L. Mentel, G. N. Kalantzopoulos, D. K. Pappas, I. Dovgaliuk, U. Olsbye, K. P. Lillerud, P. Beato, L. F. Lundegaard, D. S. Wragg, S. Svelle, *J. Phys. Chem. Lett.* **2018**, *9*, 1324–1328.
- [34] D. S. Wragg, F. L. Bleken, M. G. O'Brien, M. Di Michiel, H. Fjellvåg, U. Olsbye, *Phys. Chem. Chem. Phys.* **2013**, *15*, 8662–8671.
- [35] Y. Song, Y. Xu, Y. Suzuki, H. Nakagome, X. Ma, Z. G. Zhang, *J. Catal.* **2015**, *330*, 261–272.
- [36] E. A. Uslamin, H. Saito, Y. Sekine, E. J. M. Hensen, N. Kosinov, *Catal. Today* **2020**, 1–9.
- [37] K. Hadjiivanov, J. Saussey, J. L. Freysz, J. C. Lavalley, *Catal. Lett.* **1998**, *52*, 103–108.
- [38] K. I. Hadjiivanov, *Catal. Rev. Sci. Eng.* **2000**, *42*, 71–144.
- [39] M. Mihaylov, A. Penkova, K. Hadjiivanov, M. Daturi, *J. Mol. Catal. A* **2006**, *249*, 40–46.
- [40] J. Baltrusaitis, J. Schuttlefield, J. H. Jensen, V. H. Grassian, *Phys. Chem. Chem. Phys.* **2007**, *9*, 4970–4980.
- [41] J. B. Peri, *J. Phys. Chem.* **1982**, *86*, 1615–1622.
- [42] C. Lamberti, A. Zecchina, E. Groppo, S. Bordiga, *Chem. Soc. Rev.* **2010**, *39*, 4951–5001.
- [43] S. F. Gerasimov, V. N. Filimonov, *React. Kinet. Catal. Lett.* **1984**, *25*, 273–275.
- [44] Y. Xu, J. Wang, Y. Suzuki, Z. G. Zhang, *Appl. Catal. A* **2011**, *409–410*, 181–193.
- [45] N. Kosinov, E. A. Uslamin, L. Meng, A. Parastaev, Y. Liu, E. J. M. Hensen, *Angew. Chem. Int. Ed.* **2019**, *58*, 7068–7072; *Angew. Chem.* **2019**, *131*, 7142–7146.
- [46] V. T. T. Ha, A. Sariog˘lan, A. Erdem-Şenatalar, Y. Ben Taarit, *J. Mol. Catal. A* **2013**, *378*, 279–284.
- [47] W. Liu, Y. Xu, S. T. Wong, L. Wang, J. Qiu, N. Yang, *J. Mol. Catal. A* **1997**, *120*, 257–265.
- [48] M. Borsboom, W. Bras, I. Cerjak, D. Detollenaere, D. Glastra Van Loon, P. Goedtkindt, M. Konijnenburg, P. Lassing, Y. K. Levine, B. Munneke, M. Oversluizen, R. Van Tol, E. Vlieg, *J. Synchrotron Radiat.* **1998**, *5*, 518–520.
- [49] B. Ravel, M. Newville, *J. Synchrotron Radiat.* **2005**, *12*, 537–541.
- [50] A. Michalowicz, J. Moscovici, D. Muller-Bouvet, K. Provost, *J. Phys. Conf. Ser.* **2009**, *190*, 012034.
- [51] a) W. H. Cassinelli, L. Martins, A. R. Passos, S. H. Pulcinelli, C. V. Santilli, A. Rochet, V. Briois, *Catal. Today* **2014**, *229*, 114–122; b) A. Kurlov, X. Huang, E. B. Deeva, P. M. Abdala, A. Fedorov, C. R. Müller, *Nanoscale* **2020**, *12*, 13086–13094; c) M. Nikulshina, P. Blanchard, C. Lancelot, A. Griboval-Constant, M. Marinova, V. Briois, P. Nikulshin, C. Lamonier, *Appl. Catal. B* **2020**, *269*, 118766.
- [52] B. S. Clausen, G. Steffensen, B. Fabius, J. Villadsen, R. Feidenhans'l, H. Topsøe, *J. Catal.* **1991**, *132*, 524–535.
- [53] N. Fairely, A. Carrick, *Acolyte Sci.* **2005**, 1–177.

Manuscript received: October 28, 2021

Accepted manuscript online: November 25, 2021

Version of record online: December 16, 2021